Energy Strategy Reviews 52 (2024) 101306

Contents lists available at ScienceDirect

Energy Strategy Reviews

journal homepage: www.elsevier.com/locate/esr

A novel on intelligent energy control strategy for micro grids with renewables and EVs

Hussaian Basha CH [a], Ramakrishna Reddy K [b], Dhanamjayulu C [c,**], Innocent Kamwa [d,*], S.M. Muyeen [e]

[a] EV R&D Laboratory, NITTE Meenakshi Institute of Technology, Bengaluru, India
[b] D Y Patil International University, Pune, Maharashtra, India
[c] School of Electrical Engineering, Vellore Institute of Technology, Vellore, India
[d] Department of Electrical Engineering and Computer Engineering, Laval University, Quebec, QC G1V 0A6, Canada
[e] Department of Electrical Engineering, Qatar University, Doha, 2713, Qatar

ARTICLE INFO

Handling Editor: Dr. Mark Howells

Keywords:
Microgrid
Electric vehicles
Intelligent CNN RES
Battery degradation
G2V
EV fleet and power loss

ABSTRACT

Energy management in Micro Grids (MG) has become increasingly difficult as stochastic Renewable Energy Sources (RES) and Electric Vehicles (EV) have become more prevalent. Even more challenging is autonomous MG operation with RES since prompt frequency control is required. We provide an innovative Energy Management Strategy (EMS) for MG with grid support in this academic publication. By integrating RES and EV storage, we seek to decrease reliance on the grid. The EMS consists of three execution phases: Ranking for EV Recommendation (RER), Optimal Power Allocation (OPA) for Fleet, and EV Storage Allocation (OAES). The aim of slicing the time in to smaller in intervals is to update the energy and power scheduling in shorter intervals as per the changes are going on in the system. The period of 24 h is divided into 96 intervals (t) and storage requirements (kWh/t) are estimated based on the estimated load and RES together with the necessary storage volume. We employ three approaches that are frequently used for communication channel power allocation optimization to accomplish OAES. With two objectives: minimum network power loss plus voltage fluctuations, the Multi-Objective Optimization Problem (MOOP) is solved for each 't' based on OAES to provide the Optimal Power Flow (OPF). The Pareto-front is used to calculate the best amount of power from each fleet in each 't'. The data received from the fuzzy rule base is used in the third stage to train an intelligent Convolutional Neural Network (CNN), which has rank of EV as an output and four decision variables as inputs. The main goals in this stage are to minimize battery degradation and to make the most of it for MG support. With the aid of a MATLAB-based simulation setup and heterogeneous entities, the primary goal of EMS is examined and put into practice in an On-grid MG.

1. Introduction

The reliability of power systems with DERs, AC/DC loads, and energy storage has recently been improved using MGs. Through the use of power converters, MGs improve energy efficiency when combined with RESs like PV plants, ESSs, and EVs [1]. Using DERs and regulated loads, MG operators can profit from selling excess power and offering dependable power. To maximize profit, it is essential to have a smart EMS, an effective energy price policy, and the use of incentive programs and service markets [2]. Different optimization approaches have been used on MGs, including conventional methods as well as artificial intelligence techniques like genetic algorithms and differential evolutionary methods [3]. These methods aim to reduce the operating costs of MGs at realistic energy prices while taking into account a number of variables, including the use of grids, RES, energy storage systems, fuel stacks, and residential load demand.

For instance, a genetic algorithm was used in Ref. [4] to solve the power flow problem and to reduce the operational cost of a DC MG, and an adaptive differential evolution algorithm was proposed in Ref. [5] for the same problem. Additionally [6], concentrated on a techno-economic

* Corresponding author.
** Corresponding author.
E-mail addresses: dhanamjayulu.c@vit.ac.in (D. C), innocent.kamwa@gel.ulaval.ca (I. Kamwa).

https://doi.org/10.1016/j.esr.2024.101306
Received 20 June 2023; Received in revised form 22 October 2023; Accepted 10 January 2024
Available online 1 February 2024

analysis using smaller Hybrid RES parts to satisfy particular household power requirements. In the future years, it is projected that EVs will play a crucial role in the power grid, potentially resolving the world's fossil fuel shortage and air pollution crisis [7]. The efficient use of electric vehicles (EVs) as loads and power storage batteries coupled with renewable energy sources (RESs) can dramatically reduce emissions [8]. But when EVs are connected to the electrical grid, there are technical issues that need to be carefully handled.

A network for energy storage, EV energy monitoring, and energy delivery was suggested in Ref. [9] as a way to improve the use of recurring PV sources for charging EVs. In order to reduce the overall operating cost of the parking space, this strategy schedules EV charging and discharging to maximize the usage of energy from RES and Energy Storage System (ESS). The current study suggests the best functional methods for lowering the operating costs of microgrids (MGs), which include EVs and RES in addition to other DERs. Due to the voltage profiles' sensitivity to changes in load and DERs, low-voltage DC (LVDC) distribution systems' voltage regulation has attracted a lot of attention lately [10]. Due to its relatively low voltage (1500V DC), LVDC distribution systems are quite sensitive to changes in the electricity generated by sources like PV plants. In LVDC distribution systems, the typical range of voltage profiles is 0.82–1.10 per unit.

Researchers have suggested several voltage-control methods, including those described in Ref. [11], to address this problem. In order to determine voltage sensitivity factors (VSFs) and correct for voltage issues appropriately, these methods coordinate the principal converters and DER sprinkling in a power supply system. The working rate of DERs and total operating costs are ignored, and the voltage adjustment strategy is only applied after a voltage problem has occurred, which are some of the shortcomings of these systems. Future studies should look into more practical and effective solutions to this important problem. The addition of RESs and EVs to the power system can exacerbate current problems by increasing peak load demand and causing uncertainty [12]. The management of MGs with EVs has been the subject of numerous research, and parking lots acting as active distribution networks have shown promise in resolving this problem [13].

Appliance load adjustment and EV power trading have been made possible via a network that integrates EV aggregators and customers [14]. In the event of a power shortage, available energy from battery storage systems can be used to supply neighbouring MGs with power. Further research has been done on the possibilities of fuel cell electric vehicles (FC-EVs) in MGs [15]. Virtual power plants (VPPs) have also been studied for combined power plus standby planning, with the impact of CO2 emissions taken into account via a penalty mechanism [16]. There are opportunities when electric vehicles (EVs) are integrated into microgrids (MGs). The total load demand may fluctuate as a result of EVs, but they also offer a chance to monitor intermittent electricity produced by renewable energy sources (RESs). Long charging times are one issue with EV charging. A distributed active framework for allocating a sizeable number of EVs by taking into account many parking lots is presented in Ref. [17], while hierarchical event-driven multi--agent models have been employed to tackle the corresponding charging arrangement issue of EVs in Ref. [18]. Reference [19] suggests a scheduling issue for EVs for various parking lots assigned to the electricity system and supplied by RES. Due to the bidirectional power flow, V2G systems can be difficult to control and stable. In order to protect the battery and extend its longevity, it is critical to correctly monitor and control the battery's level of charge in V2G systems.

In a trailblazing series of studies, researchers explored multifaceted aspects of energy solutions. Study [20] delved into transactive energy dynamics, while [21] optimized microgrids with diverse resources, ensuring resilience [22]. pioneered consumer-centric microgrids, balancing tech and economics. Additionally [23], provided vital sizing guidelines for hybrid renewable systems. Study [24] focused on microgrid operations, optimizing switching mechanisms for enhanced voltage profiles. Meanwhile [25], tackled vehicle-to-grid technologies, reducing costs and emissions while stabilizing networks. In the realm of electric vehicles [26], optimized vehicle-to-grid technologies, meticulously balancing operational costs and emissions.

Further innovations emerged with Study [27], integrating hydrogen storage with photovoltaics for emerging electricity markets. Study [28] proposed a real-time cooperative system for hybrid microgrids, guaranteeing energy supply while lowering market prices. Simultaneously [29], revolutionized district heating site selection, optimizing energy costs with GIS-based tools. Lastly [30], introduced an innovative Energy Management System with a Multi-Agent System, optimizing energy utilization in neighbourhood grids. Together, these studies exemplify the cutting edge of sustainable energy research.

The quality of the power in the grid may be impacted by the high amounts of harmonics and voltage fluctuations that EV power may produce. Despite the fact that V2G and G2V may result in more charging and discharging cycles, which may hasten battery deterioration, a well-designed battery management system and suitable charging rates can help to lessen these adverse impacts. A comprehensive strategy for controlling energy in MGs with RES and EV/fleet storage is provided by the proposed EMS. With EVs acting as virtual storage units, the EMS seeks to decrease reliance on the grid and enhance the use of renewable energy sources. This method has the potential to increase grid stability and energy efficiency while promoting environmental cleanliness. The power handling of MGs with EVs and RES is therefore improved, which is a positive finding.

The EMS operates in three stages.

Stage I. Optimal Allocation EV Storage (OAES)

Objective: Load flattening to reduce grid dependency.

Method: Utilizes common techniques for optimal power allocation in communication channels.

Stage II. Optimal Power Allocation (OPA) for Fleet

Based on OAES, solves a Multi-Objective Optimization Problem (MOOP) for each 't.'

Objectives: Minimize network power loss and voltage fluctuations.

Determines the optimal power allocation from each fleet on the Pareto-front.

Stage III. Ranking for EV Recommendation (RER)

Employs an intelligent Convolutional Neural Network (CNN) trained with data from a fuzzy rule base.

Inputs: Four decision variables; Output: Rank of EV.

Objectives: Minimize battery degradation and maximize utilization for MG support.

The main features of the proposed study that stand out as innovative include.

- Optimal EV storage utilization by predicting OAES using three alternative approaches in each interval of the provided zone.
- Optimal power allocation (OPA) for fleets to reduce voltage swings and network power loss.
- With four decision variables that affect how well EV storage is used and how quickly battery life degrades, a fuzzy controller is used to determine ranks for EVs in each t.
- Intelligent CNN selection of EVs by ranking, where the training data is generated from the synthetic data (fuzzy rule base).
- In addition to voltage profiles, many scenarios have been used to examine grid energy costs and EV battery longevity.

Assumptions.

✓ Fleets are treated as three-phase loads, therefore load imbalance is not taken into account. It is assumed that EV fleets had been positioned ideally in the MG.

✓ Phase load imbalances caused by single-phase residential charging have not been taken into account.

- ✓ Owners of EVs consented to MG assistance in exchange for certain incentives and a pre-request for EV charging when traveling.
- ✓ Due to the low X/R ratio, the effect of active power flow on voltage control is taken into account.
- ✓ It is expected that the MG's communication configuration has been built for the flow of data and control.

The key factor here is EV as virtual storage unit avoiding additional expenditure on fixed storage systems for energy management. However, EV as a virtual storage unit involves lot of constraints out of which we address some of the key constraints such as battery degradation, economical benefit and owner flexibility.

The remaining of this article includes the following: in section 2 EV mobility model is presented, in section 3, cost calculations for energy is discussed followed by section 4 which explains about state of health of the battery. Section 6 is dedicated for proposed energy management strategy. Section 6 is dedicated for optimal Allocation EV Storage followed by section 7 that explains about MOOP formulation for OPA and section 8 is dedicated for smart selection of EVs and finally in section 9, results and insights are discussed.

2. Modelling of EV mobility

2.1. EV mobility model

In this work, we take into account two EV use cases: EVs residing at home and EVs residing in the Fleet. Initially, a straightforward probabilistic method is used to estimate, without accounting for any uncertainty, the likelihood that a vehicle will be available at home. However, this uncertainty is later taken into account in the plug-in electric vehicle (PEV) availability prediction. The charging of PEVs outside of the home, which is supposed to happen due to unanticipated trip extensions, is not taken into consideration. It is confirmed that in this investigation, the needed State of Charge (SoC) and the amount of charge in the battery before the trip begins are both always set at 0.8. Scheduling PEVs for grid support requires an accurate estimation of their availability. In order to do this, PEV mobility models are utilized, which report on the preparedness of the vehicles for grid support depending on their state of charge level and current idle time. In this study, the PEV mobility model is developed using data from the British National Travel Survey (NTS). Estimating the total amount of energy that can be stored by all EVs is required to provide V2G support, whereas figuring out the storage capacity of each EV is necessary to enable G2V support. However, because of the uncertainty around EV availability and the level of energy consumption brought on by unforeseen journey itineraries, precisely calculating this during EV scheduling can be difficult. Let's say a PEV has a low SoC status and is predicted to stay at the residence in a discharge zone for a long time. In that situation, it would be wise to plan the vehicle for a later time in the same zone. This plan makes sure that the PEV's available energy is used effectively and, when necessary, contributes to grid assistance.

$$\mathrm{SoC}_{\mathrm{i,ev}}^{\mathrm{new}} = \mathrm{SoC}_{\mathrm{i,ev}}^{\mathrm{old}} - \left(\mathrm{S}_{\mathrm{i,ev}}^{\mathrm{old}} - \gamma \mathrm{l}\right) \Big/ \mathrm{S}_{\mathrm{ev}}^{\mathrm{cap,i}} \tag{1}$$

$\mathrm{SoC}_{\mathrm{I,ev}}^{\mathrm{new}} =$ SoC after traveling of length

$\mathrm{SoC}_{\mathrm{i,ev}}^{\mathrm{old}} =$ SoC before travel

$\mathrm{SoC}_{\mathrm{ev}}^{\mathrm{cap,i}} =$ EV battery capacity (kWh)

Overall, Equations (2) and (3) offer a trustworthy way to identify the SoC stages of PEVs engaged in grid repair. This strategy is required to guarantee the grid support capabilities and efficacy of PEVs over the long run. For Case discharging, and charging cases,

$$\mathbf{SoC}_{\mathbf{i,ev}}^{\mathbf{t+1}} = \mathbf{SoC}_{\mathbf{i,ev}}^{\mathbf{t}} - \left(\mathbf{S}_{\mathrm{ev}}^{\mathbf{t,i}} - \mathbf{S}_{\mathrm{pev}}^{\mathbf{t+1,i}}\right) \Big/ \mathbf{S}_{\mathrm{ev}}^{\mathbf{cap,i}} \tag{2}$$

$$\mathrm{SoC}_{\mathbf{i,ev}}^{\mathbf{t+1}} = \mathbf{SoC}_{\mathbf{i,ev}}^{\mathbf{t}} + \left(\mathbf{S}_{\mathrm{ev}}^{\mathbf{t+1,i}} - \mathbf{S}_{\mathrm{ev}}^{\mathbf{t,i}}\right) \Big/ \mathbf{S}_{\mathrm{ev}}^{\mathbf{cap,i}} \tag{3}$$

$\mathrm{SoC}_{\mathbf{i,ev}}^{\mathbf{t+1}} =$ **SoC in the interval** $'\mathbf{t}+\mathbf{1}'$

$\mathrm{SoC}_{\mathbf{i,ev}}^{\mathbf{t}} =$ **SoC in the interval** '**t**'

The laxity of PEV is indicated in intervals by Equations (4) and (5). A higher laxity suggests that the vehicle will be more flexible in providing grid support, whereas a lower laxity suggests that the vehicle would be less flexible. The laxity value is determined depending on a number of variables, including the current SoC, target SoC, departure time, maximum power rate, and capacity of the battery. So when employing EV storage to support the grid, it is an important factor to take into account. Notably, the goal SoC is set at 0.8 for all EVs.

$$\mathrm{L}_{\mathrm{ev}}^{\mathrm{i,t}} = \mathrm{t}_{\mathrm{d}}^{\mathrm{i}} - \mathrm{t} - \mathrm{T}_{\mathrm{ch}}^{\mathrm{i}} \tag{4}$$

$$\mathrm{L}_{\mathrm{ev}}^{\mathrm{i,t}} = \mathrm{t}_{\mathrm{d}}^{\mathrm{i}} - \mathrm{t} - \frac{\left(\mathrm{SoC}_{\mathrm{ev}}^{\mathrm{i,t=t_d}} - \mathrm{SoC}_{\mathrm{ev}}^{\mathrm{i,t}}\right)\mathrm{S}_{\mathrm{ev}}^{\mathrm{i,cap}}}{\eta \mathrm{P}_{\mathrm{rate}}^{\mathrm{i,t}}} \tag{5}$$

$\mathrm{SoC}_{\mathrm{ev}}^{\mathrm{i,t=t_d}} =$ SOC required by the time of departure

$\mathrm{t_d} =$ time of depature (interval)

$\mathrm{P}_{\mathrm{rate}}^{\mathrm{i,t}} =$ C rate (kW)

2.2. Estimation of storage capacity

(i) EVs staying at the residence

In order to avoid any delays to the journey schedule, the utility must guarantee that the EV's target SoC is maintained before it departs. Laxity is a measure of the SoC's degree of flexibility and the length of the grid support period. It is carefully monitored to make sure the SoC stays at the upper limit of 0.8 before the EV's departure time interval of 96. However, the SoC is anticipated to have run out once the car returns from its trip because of energy use. Eq. (6) is used to calculate the total amount of storage space for EVs currently available for charging in zone z. Eq. (7) is also applied to estimate the total energy presented for discharging in the same zone. At the beginning of each interval in the zone, the value of E_ev^(cap, i) is assessed. It's a prevalent misconception that employers have readily accessible electric vehicle fleets that are parked there all day. Researchers have examined mobility data to assess the availability of these vehicles and their capability for V2G and G2V operations. Probability density functions have been derived by looking at historical data on EV arrival and departure.

$$S_{ev}^{g2v} = \sum_{i=1}^{x+y} \left\{0.9 * S_{ev}^{cap,i} - S_{ev}^{i,t}\right\} * p_{avail}^{i,t} \tag{6}$$

$$S_{ev,t=1}^{v2g} = \sum_{i=1}^{y} \left\{S_{ev}^{i,t} - 0.2 * S_{ev}^{i,cap}\right\} * p_{avail}^{i,t} - \sum_{i=1}^{x} \left\{S_{ev}^{i,t=td} - S_{ev}^{i,t}\right\} \tag{7}$$

$S_{ev,z}^{g2v} =$ *Storage available for G2V*

$S_{ev,z}^{v2g} =$ *Storage available for V2G*

$S_{ev}^{i,t} =$ *Storage available in* i^{th} *EV*

(ii) EVs staying in fleet

For a given day of the week, in the tth time, the possibility of ith EV coming is $\mathrm{p}_{\mathrm{i,t}}^{\mathrm{a}}$ plus that of for retreat is $\mathrm{p}_{\mathrm{i,t}}^{\mathrm{d}}$. The CDFs are $\mathrm{p}_{\mathrm{i,t}}^{\mathrm{a,c}}$ and $\mathrm{p}_{\mathrm{i,t}}^{\mathrm{d,c}}$ for arrival and departure respectively.

Table 1
Structure of grid tariff.

Power Range	Cost (Rs.)	Tariff category
0 to 80 % of $P_{max}^{g,kVA}$	$P_{max}^{g,kVA} * 0.8 * 475$	Fixed price
80 to 100 % of $P_{max}^{g,kVA}$	$P_{max}^{g,l} * 475$	Semi-Fixed price
> 100 % of $P_{max}^{g,kVA}$	$P_{max}^{g,l} * 475 + P_{extra}^{g,l} * 475$	With penalty price
0 to 7000 kWh	$7000 * C_e^g$	Fixed price
> 7000 kWh	$U_e^g * C_e^g$	Variable price

$$p_i^j = p_{i,t}^{a,c} - p_{i,t}^{d,c} \tag{8}$$

L is defined as EV's vector is represented by (9)

$$L = [\, l_1 l_2 l_3 \ldots\ldots\ldots\, l_N] \tag{9}$$

SoCs at the time of arrival are given by (10).

$$SoC_{ev}^{arr} = M \,/\, C\, [\, l_1 l_2 l_3 \ldots\ldots\ldots\, l_N] \tag{10}$$

A dip in SoC is expected for consumption for the trip (11).

$$SoC_{i,ev}^{new} = SoC_{i,ev}^{old} - \left(E_{ev}^{old,i} - \gamma l\right) \Big/ E_{ev}^{cap,i} \tag{11}$$

Here, $SoC_{i,ev}^{new}$ is nothing but $SoC_{i,ev}^{arr}$.

The SoC levels updated after each interval are as follows for V2G and G2V.

$$SoC_{i,ev}^{t+1} = SoC_{i,ev}^{t} - \left(S_{ev}^{t,i} - S_{ev}^{t+1,i}\right) \Big/ S_{ev}^{cap,i} \tag{12}$$

$$SoC_{i,ev}^{t+1} = SoC_{i,ev}^{t} + \left(S_{ev}^{t+1,i} - S_{ev}^{t,i}\right) \Big/ S_{ev}^{cap,i} \tag{13}$$

Available storage for G2V and V2G is given by (14) and (15) from each EV.

$$e_{i,j}^{g2v} = p_i^j * C * \left(1 - SoC_i^j - 0.2\right) \tag{14}$$

$$e_{i,j}^{v2g} = p_i^j * C * \left(SoC_i^j - 0.2\right) \tag{15}$$

Total available storage for G2V and V2G is given by (16) and (17).

$$S_{ev,z}^{g2v} = \left[s_i^{1,g2v} s_i^{2,g2v} s_i^{3,g2v} \ldots\ldots\ldots\ldots s_i^{N,g2v}\right] \tag{16}$$

$$S_{ev,z}^{g2v} = \sum_{j=1}^{N} e_i^{j,g2v} \tag{17}$$

$$S_{ev,z}^{v2g} = \left[s_i^{1,v2g} s_i^{2,v2g} s_i^{3,v2g} \ldots\ldots\ldots\ldots s_i^{N,v2g}\right] \tag{18}$$

$$S_{ev,z}^{v2g} = \sum_{j=1}^{N} s_i^{j,v2g} \tag{19}$$

3. Cost of grid power

The state of the location, the DISCOM serving the area, the type of institution, and the electricity consumption all play a role in determining the energy rate for educational institutions in India. Schools are typically billed at higher rates than residential customers since they are considered commercial or industrial clients. The three-part tax model used in India's energy tariff structure combines a fixed cost (a), a semi-fixed cost (b), and a variable cost (c). Table 1 presents the tariff structure for easy comprehension. Let the maximum demand that is authenticated with utility ($P_{max}^{g,kVA}$) be 850kVA. There will be a minimum demand up to which it is fixed is 80 % of $P_{max}^{g,d}$ which is shown below.

0–80 % of $P_{max}^{g,kVA}$, the price is $P_{max}^{g,kVA} * 0.8 C_d^g$ (Fixed Cost).

80–100 % of $P_{max}^{g,kVA}$, the price is $P_{max}^{g,l} * C_d^g$ (Semi-Fixed Cost).

> 100 % of $P_{max}^{g,kVA}$, the price is $P_{max}^{g,l} * C_d^g + P_{extra}^{g,l} * C_d^g$ (With penalty).

Where, $P_{max}^{g,l}$ is the extreme power consumed by the utility grid.

The total price of consumed power from the grid in a month (C_T^g) is determined by Eq. (21).

$$\text{Power cost of grid} = \text{Fixed cost} + (\text{Semi} - \text{fixed cost}) + \text{Varying cost} + \text{Penalty}$$

$$C_T^g = \left\{P_{max}^{g,kVA} * 0.8 * 475 + 7000 * C_e^g\right\} + \left\{P_{max}^{g,l} * 475\right\} + \left\{U_e^g * C_e^g + P_{max}^{g,l} * 475\right\} + \left\{P_{extra}^{g,l} * 475\right\} \tag{20}$$

4. State of health modelling

Particularly when it comes to defining the phrase "state of health" (SoH), the field of battery health is difficult to understand. Based on the unique usage circumstances of the battery, the definition of SoH can vary significantly. An approach for calculating cell state of health in terms of capacity loss as a function of temperature and SoC is put forth by Long Lam, a specialist in circuit-based Li-Ion battery models [31]. He contends that C-rates, which are frequently used to gauge battery discharge and charge rates, have little bearing on battery aging at room temperature and should not be taken into account for estimating SoH. Experiments support Lam's assertion that the impact of C-rate on cell deterioration is outweighed by the temperature increase brought on by Ohmic heating. Lam's research does not model this phenomenon because there are insufficient experimental data and the presumption that the battery management system (BMS) in an electric vehicle (EV) will take care of the problem, even though high C-rates can accelerate battery degradation at low temperatures.

A cell will also inevitably deteriorate with time as a result of calendar aging. An aging model based on the Arrhenius equation is described in Ref. [32] and takes into account changing operating conditions over time, despite the fact that this type of aging is frequently less explored in the literature than aging caused by cycling. The 80 % limit is generally employed in EV applications, even if the definition of SoH may vary based on the particular application. A battery cell loses power as it ages because its internal resistance rises. Even though it might be more important for identifying a battery's health when employed in hybrid electric vehicle (HEV) applications, this factor isn't covered as much in the literature as capacity loss. Equation (21) [33] gives the definition of the state of health that is employed in this thesis.

$$SoH = \left(1 - S_{loss} \,/\, 0.2 * SoC_{ev}^{cap,i}\right) \tag{21}$$

$$S_{loss} = S_{loss}^{cal} + S_{loss}^{cyc} \tag{22}$$

(i) Cycle Aging

A method is used to model aging-induced capacity fading and heat deterioration where aging parameters are consistent within each event. Thermal degradation is modeled using the Arrhenius equation with an empirical coefficient, which takes into account cell temperature, reference temperature, activation energy, and gas constant. An average state of charge over event I, the state of charge normalized deviation, and model parameters are all included in the empirical coefficient. Equation (23), which is calculated, is utilized to determine cycling-induced capacity fade.

$$S_{loss}^{cyc} = \sum_{t=1}^{n} \left\{\propto_1 \Delta SoC_t e^{(\propto_2 SoC_{mean})} + \propto_3 e^{(\propto_4 \Delta SoC_t)}\right\} e^{\left\{-\frac{\partial}{r}\left(\frac{1}{T_t} - \frac{1}{T_{ref}}\right)\right\}} C_t \tag{23}$$

(ii) Calendar Aging

Here, a span of time is referred to as an event. 1000 s have been

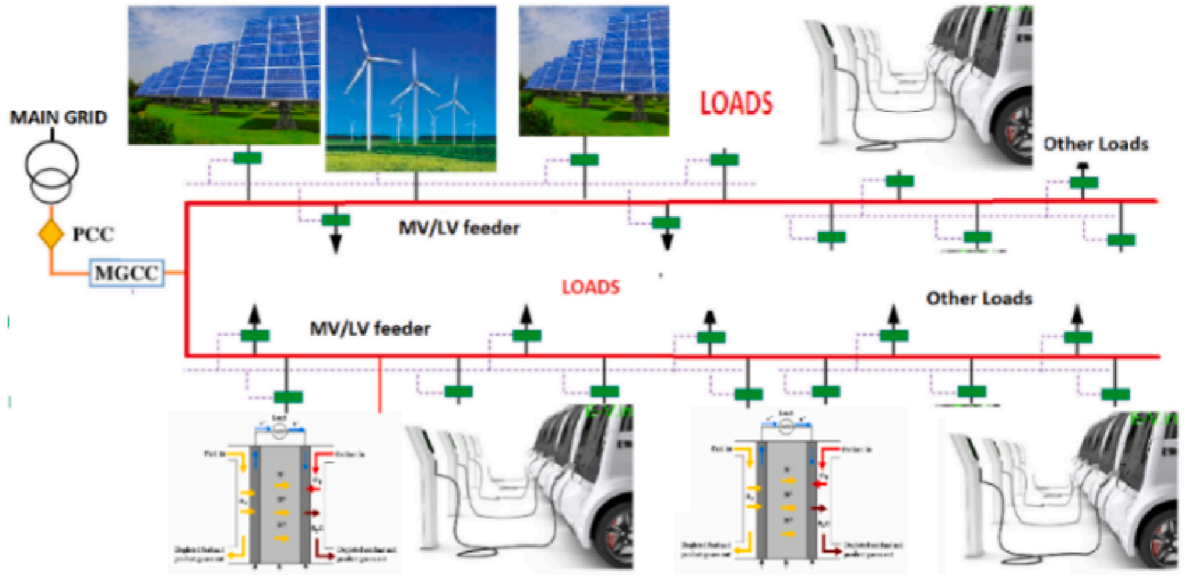

Fig. 1. Block diagram of Micro Grids.

arbitrarily chosen as the ad hoc value for each simulation because it seems to adequately reflect temperature and state of charge dynamics. To establish a suitable event time and assess whether there are better triggers for events than just time, such as SoC (Eq. (24)), it would be more appropriate to carry out experimental testing on battery cells.

$$\frac{dS_{cal}}{dt} = \mu(T, SoC)\left\{1 + S_{cal}(t)/S_{cap}\right\}^{\theta} \tag{24}$$

$$\mu(T, SoC) = \beta_1 e^{\left\{\frac{e_1}{r}\left(\frac{1}{T}-\frac{1}{T_{ref}}\right)\right\}} SoC + \beta_2 e^{\left\{\frac{e_2}{r}\left(\frac{1}{T}-\frac{1}{T_{ref}}\right)\right\}} \tag{25}$$

dS_{cal} = change in calendar life

5. Proposed energy management strategy

Fig. 1 displays the chosen energy management technique. The network power losses can be calculated as "Energy Input at the Bus (kWh)-Actual Energy Billed (kWh))/Energy Input (kWh) x100". Additionally, the load factor is calculated as "average load over a specific time period divided by peak load simultaneously." Increasing the load utilization factor reduces energy losses, hence in our work, we concentrate on this in terms of load flattening. We suggested an innovative and practical approach to energy management in MGs enhanced by grid support. By utilizing RES and EV storage, the main goal is to reduce the MG's reliance on the grid. The three unique stages of our suggested EMS's operation are OAES, OPF, and RER. We use three widely used techniques for communication channel power allocation optimization to achieve OAES. Based on OAES, OPF is gained by resolving a MOOP with two goals in mind: to reduce voltage variation and network power loss. With the use of this method, we can compute the Pareto-front's ideal power output from each fleet for each time interval (t).

The proposed EMS is designed to divide a day into 96 times (t), and the expected load and RES are used to determine how much storage is required (kWh/t). We determine the required amount of storage as well as the charging and discharging temporal zones. The main objective of this EMS is to accomplish "load flattening," which will lessen the MG's dependence on the grid. The data we have obtained from the fuzzy rule base is used to train an intelligent CNN in the final step of our EMS strategy. This CNN comprises four decision factors as inputs and outputs a ranking of the EV. The main goals of this stage are to reduce battery deterioration and increase its capacity for MG support. The main goals of this stage are to reduce battery deterioration and increase its capacity for MG support. Our work includes numerous case studies to analyse the effectiveness of the proposed EMS, which we have implemented in a MATLAB-based smart grid configuration with heterogeneous entities. The flowchart (Fig. 2) shows the proposed approach's entire flow diagram for ease of comprehension.

6. Optimal allocation EV storage

The following three strategies have been used to achieve OAES after taking into account the energy required in each zone's intervals and the maximum available/useable energy from EVs in that zone. In order to limit the deviation from the certified maximum demand from the grid mains, we first define zones and intervals as well as the amount of power/energy required from EVs. Figs. 3–5 show the real load demand profile as well as the aforementioned power energy requirements for EVs. The best quantity of energy that may be used from EVs in the allotted period has been determined for each zone using the three optimization approaches. OPA will be selected for each fleet at the given time interval after OAES is determined for the specified time interval.

6.1. Iterative Water-Filling Algorithm (IWFA)

To maximize the overall utilization of EV storage, the Iterative Water-Filling Algorithm [34] is a strategy used to increase EV storage distribution among various intervals in the given zone. The water level is first estimated by the algorithm, which then iteratively updates it until convergence. Each interval's energy allocation is represented by the water level, and the intervals with higher capacity receive more energy.

6.1.1. Pseudo-code for the iterative water-filling algorithm

1 Initialize the water level λ to a small positive number
2 Set a convergence threshold ϵ
3 While not converged do:
  a Compute the capacity of each interval as a function of λ
  b Sort the intervals in decreasing order of capacity
  c Compute the water level λ as a function of the sorted intervals
  d If |λ_new - λ_old| < ϵ, exit the loop
4 Allocate energy to each interval proportional to its water level

Here, the water level or energy allocation is denoted by λ, while the

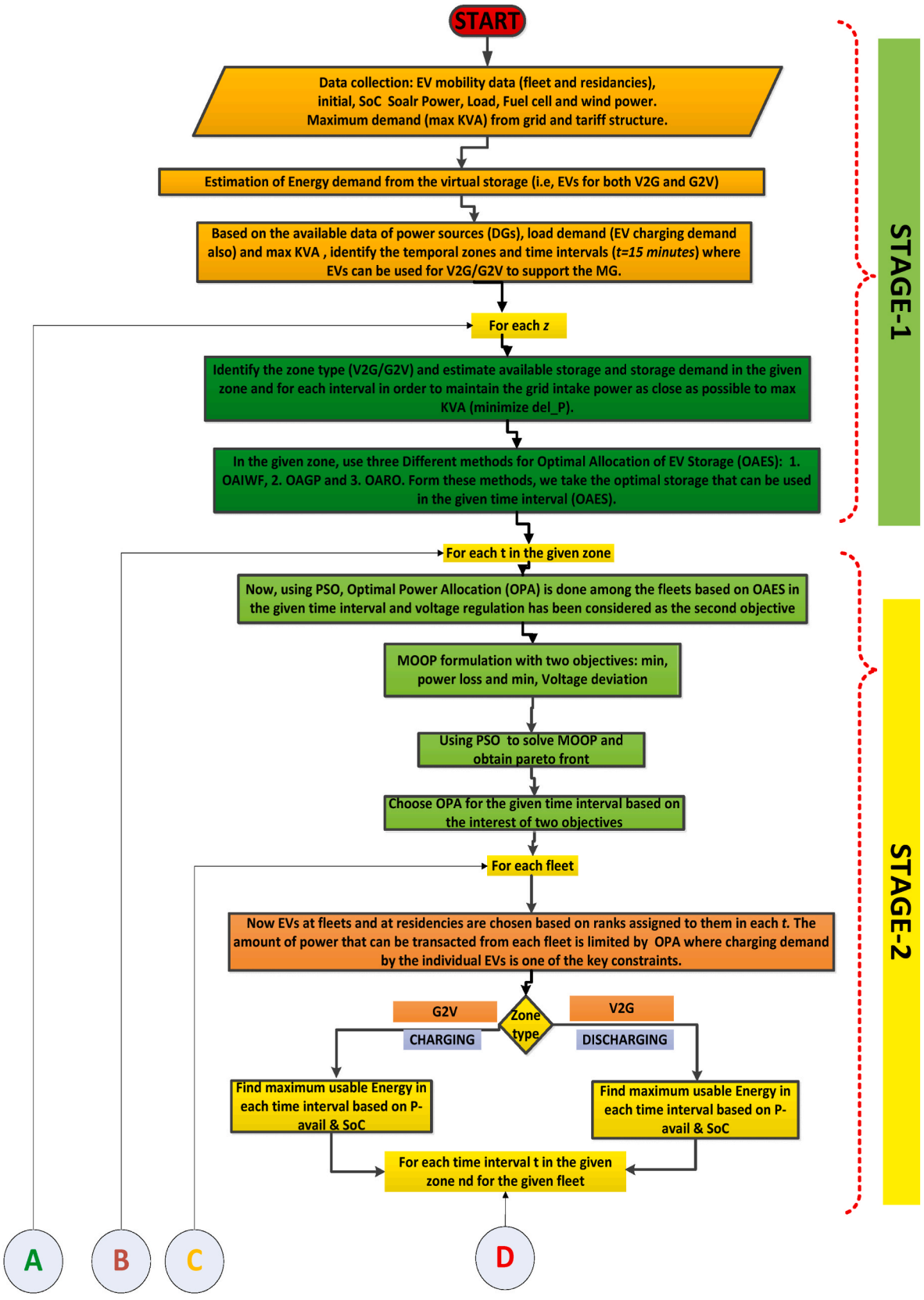

Fig. 2. Flowchart representation of proposed EV control strategy for MG EMS

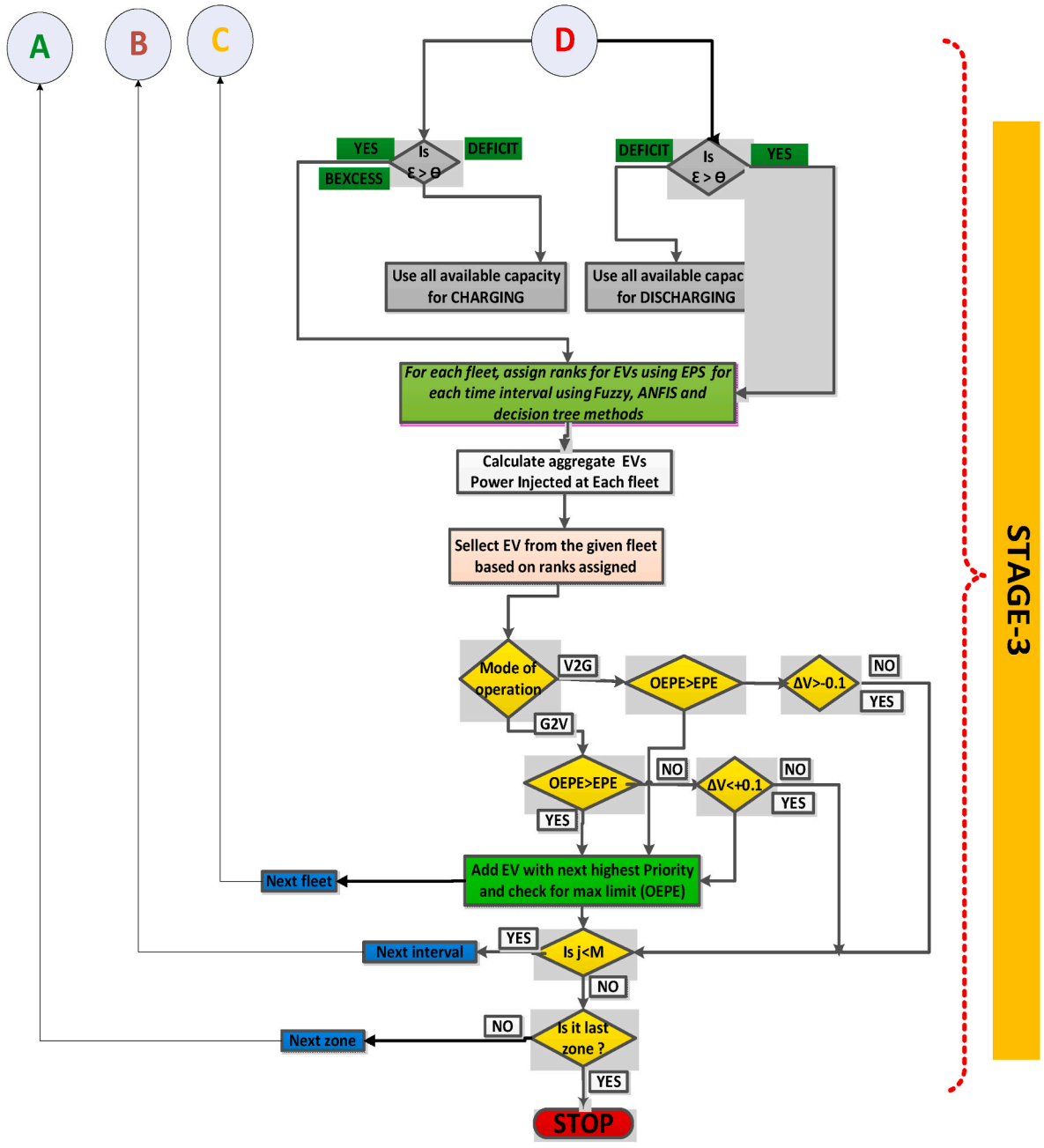

Fig. 2. (*continued*).

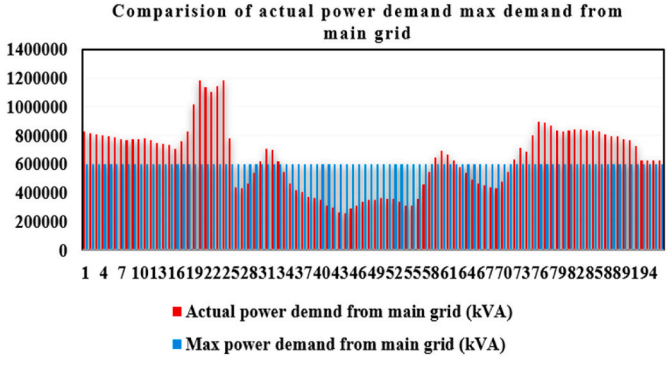

Fig. 3. Comparison of actual power demand max demand from the main grid.

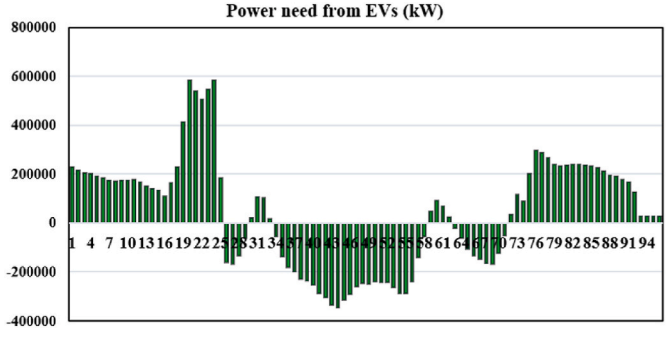

Fig. 4. Power need from EVs.

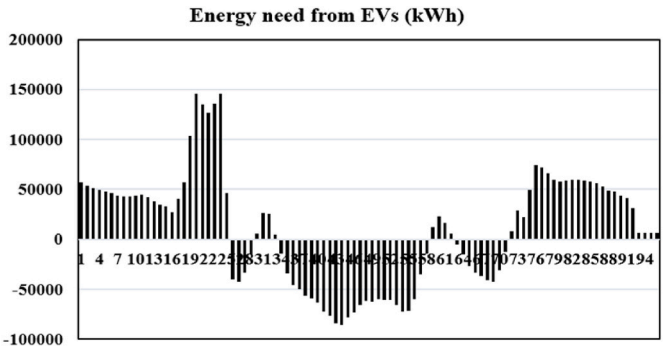

Fig. 5. Energy needs from EVs.

convergence threshold is denoted by ϵ. Each interval's capacity is calculated as a function of λ, and the intervals are then arranged in decreasing order of capacity. The algorithm then iterates until convergence, updating the water level λ depending on the sorted intervals. And finally, energy is distributed proportionally to each interval's water level.

(ii) genetic programming (GP)

Genetic operators like mutation and crossover are used to evolve the population over several generations in genetic programming, which has as its fundamental premise the creation of a population of potential solutions (referred to as "individuals") for a problem. Every individual in the population represents a potential solution to the problem, and each one's fitness is assessed according to some objective function that gauges how well it resolves the issue. We must first specify the individual representation and the fitness function before we can employ genetic programming for energy allocation. The fitness function gauges the system performance in this scenario where the person represents the energy allocated to each interval.

6.1.2. Pseudo code for energy allocation using genetic programming

Define the representation of a person's chromosomes, such as a binary string where each gene reflects the energy allotted to a particular interval.

1 Initialize: Create a random population of individuals with binary chromosomes representing energy allocation intervals.
2 Evaluate Fitness: Determine fitness values for each individual in the population.

6.1.3. Repeat until convergence

a Selection: Choose parents via tournament selection.
b Reproduction: Generate offspring using genetic operators (mutation and crossover).
c Fitness Evaluation: Assess the fitness of the offspring.
d Replacement: Replace the weakest individuals in the population with the offspring.

7. Result: return the best individual (highest fitness) as the energy allocation solution

To develop a comprehensive algorithm, many details (such as selection and genetic operators) would need to be filled in. The fitness function and chromosome representation would also need to be adjusted for the particular zone under consideration.

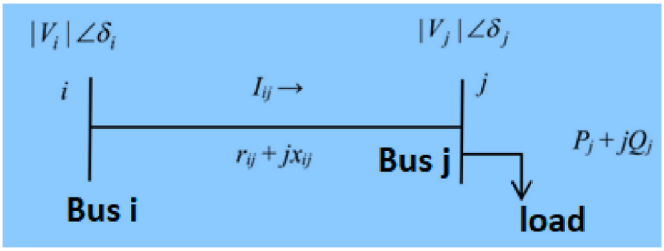

Fig. 6. Single-line bus diagram.

7.1. Robust optimization (RO)

The objective is to distribute energy among different intervals in a way that maximizes the amount of energy used by EVs overall while satisfying energy consumption and capacity limits. resistant optimization [35], which takes into consideration the uncertainty in interval circumstances and offers a solution that is resistant to variations in these variables, is one method for overcoming this challenge.

7.2. Pseudo code for energy allocation using robust optimization

1 Initialize parameters: uncertainty set, decision variables, constraints, objective function.
2 Define uncertainty scenarios considering variations in demand, supply, or other factors.
3 For each scenario in the uncertainty set:
  a) Formulate and solve the robust optimization problem with the given scenario.
  b) Store the obtained solution for the current scenario.
4 Evaluate the worst-case scenario solution, considering the most adverse outcome.
5 While worst-case solution does not meet constraints:
  a) Adjust uncertainty set or other parameters to increase robustness.
  b) Recalculate worst-case scenario solution.
6 Return the final robust optimal solution for energy allocation.

8. MOOP formulation for OPA

In this section, two objectives $min(p_{loss})$ and minimum $min(\nabla V)$ are formulated as MOOP problems that can be solved using PSO. Here, we are given a range of OPA solutions from which the MG operator may select one. It is expected that fleets and DGs are positioned strategically throughout the network. Power loss is still significantly influenced by the quantity of power that is exchanged between the fleet and grid/MG, though. By determining OPA for each fleet based on which EVs will participate in grid support, this issue is addressed.

8.1. Minimize power loss

Fig. 6 shows a single-line diagram with two buses. Here, the goal is to lower the distribution network's overall active power dissipation, which is provided by Eq. (26). Intelligent CNN for EV Recommendation (RER) is shown in Fig. 7).

$$F_1 = \min\left(P_{loss}\right) \tag{26}$$

where P_{loss} represents the system's overall active power loss, which can be calculated as follows [42]:

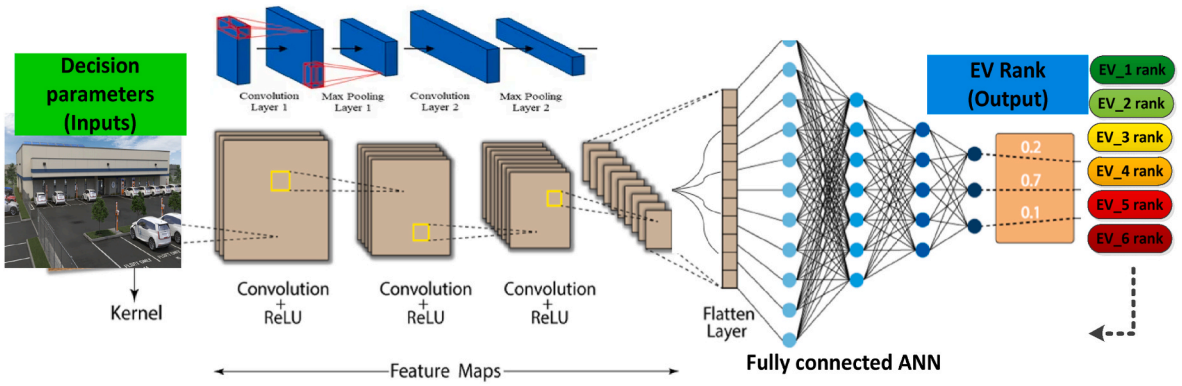

Fig. 7. Block diagram of CNN for RER.

$$P_{loss} = \frac{r_{ij}}{V_i V_j}\left(\sum_{i=1}^{N}\sum_{j=1}^{N}\cos(\delta_i - \delta_j)(P_i P_j - Q_i Q_j) + \sin(\delta_i - \delta_j) * (Q_i P_j - P_i Q_j)\right) \quad (27)$$

$\delta_i - \delta_j =$ phase angle difference $\frac{b}{w}$ bus i plus j

$V_i, V_j =$ voltages at i and j

$P_i, P_j, Q_i, Q_j =$ active plus reactive powers at i & j

In this section, two MOOP-based objectives min, (P_{loss}) and min, ΔV, that can be handled with PSO are introduced. The outcome of this procedure is a collection of OPA solutions from which the MG operator may choose. Fleets and Distributed Generations of DGs are presumptively positioned in the network's most advantageous areas. The amount of power exchanged between fleets and the grid or MG still has a significant impact on power loss, though. The OPA for each fleet is established based on which EVs will engage in grid support in order to handle this issue. While ensuring that EVs effectively participate in grid support activities, power loss and voltage fluctuations in the MG system can be reduced by optimizing the power allocation approach.

8.2. Minimize voltage deviation

This objective function is to enhance the voltage profile expressed as:

$$F_2 = \min(\Delta V) = \min\left(\sum_{i=1}^{N}(V_i - V_{rated})^2\right) \quad (28)$$

V_{rated} is the rated voltage (1.0 p.u.) and V_i is the voltage magnitude at bus i, where V is the overall voltage variations. The derived power flow equations are,

$$P_{g,i} - P_{l,i} = |V_i|\sum_{j=1}^{N} Y_{i,j} V_j \cos(\delta_i - \delta_j - \theta_{i,j}) \quad (29)$$

$$Q_{g,i} - Q_{l,i} = |V_i|\sum_{j=1}^{N} Y_{i,j} V_j \sin(\delta_i - \delta_j - \theta_{i,j}) \quad (30)$$

The extreme useable power for V2G must be kept below the total sum of the maximum power rates of all EVs, it must be ensured.

$$P_{ev}^{t,ch} \le \sum_{i=1}^{k} P_{ev}^{t,i,c} \quad (31)$$

$$P_{ev}^{t,dc} \le \sum_{i=1}^{1} P_{ev}^{t,i,dc} \quad (32)$$

Grid apparent power grid should not exceed its verified/max demand, according to a constraint.

$$\sqrt{\left(P_{grid}^{t} + Q_{grid}^{t}\right)^2} \le P_{max}^{g,kVA} \quad (33)$$

$P_{grid}^{t}, Q_{grid}^{t}$ are active and reactive powers from grid mains at time interval 't'.

Constraint on fuel cell power: P_{fc}^{t} should lie between high plus low charge limits.

$$P_{fc}^{t} \le \sum_{i=1}^{x} P_{fc}^{i,max} \quad (34)$$

$$P_{fc}^{t} \ge \sum_{i=1}^{x} P_{fc}^{i,min} \quad (35)$$

$P_{fc}^{i,max}$ = Maximum power output from ith FC.
$P_{fc}^{i,min}$ = Minimum power output from ith FC.

Battery level restrictions: Considering battery deterioration, it is preferable to maintain the battery level in a specific manner to ensure battery longevity.

$$\Phi_{min} S_{ev}^{i,cap} \le S_{ev}^{t,i} \forall t \in \{1\ldots96\} \quad (36)$$

$$S_{ev}^{t,i} \le \Phi_{max} S_{ev}^{i,cap} \forall t \in \{1\ldots96\} \quad (37)$$

Here, $S_{ev}^{i,cap}$ = Full capacity if ith battery. Φ_{min} and Φ_{max} are low, plus a high percentage of battery levels to be continued to maximize battery life.

Limits on EV power: It is important to keep in mind that EV power charges cannot exceed the battery SoC limits in the time allotted.

$$\frac{1}{\mu_{dc}} P_{ev}^{t-1,i,dc} dt \le \left(S_{ev}^{t-1,i} - \Phi_{min} S_{ev}^{i,cap}\right); \forall t \in \{1\ldots96\} \quad (38)$$

$$\mu_{ch} P_{ev}^{t-1,i,ch} dt \le \left(\Phi_{max} S_{ev}^{i,cap} - (S_{ev}^{t-1,i})\right) \quad (39)$$

Φ_{min}, Φ_{max} minandmaxSoClimits

8.2.1. Pseudo code for OPA using PSO

1 Initialize swarm with random power allocation values for EV fleets.
2 Calculate line losses for each particle in the swarm.
3 Set pbest for each particle to its initial position.
4 Set gbest to particle with lowest line losses.

5 Set max_iter and inertia weight w.
6 Repeat for each iter from 1 to max_iter:
a) For each particle i:
i Update velocity vector:
- Calculate cognitive component (c1 * rand() * (pbest_i - pos_i))
- Calculate social component (c2 * rand() * (gbest - pos_i))
- Update velocity (vel_i = w * vel_i + cognitive + social)
ii Update position vector:
- Update position (pos_i = pos_i + vel_i)
- Enforce power limits of the fleets
iii Calculate line losses for updated position.
iv If new line losses are lower than previous:
- Update pbest_i to new position
- If new line losses are lower than gbest:
- Update gbest to new position
b) Update inertia weight (w = w_max - ((w_max - w_min) * iter/max_iter))
7 Return gbest as the optimal power allocation (OPA) among fleets.

9. RER using an intelligent CNN

DoD, STP, PoP, and Laxity are decision factors for RER that are inputs to the intelligent CNN. We discuss these choice variables and their significance in determining RER in this section. We take the effect of DoD and STP into consideration to account for battery longevity. In this case, STP denotes the possibility of a transition between V2G and G2V. The DoD and STP will take care of battery longevity, therefore merely taking these two into account when making decisions will diminish the usefulness of using EV storage for MG support. PoP and Laxity, on the other hand, will act in the reverse manner and favour MG to maximize consumption. Leverage battery degradation is caused by the effects of increasing DoD and SoC. It is not advisable for an EV with a higher STP value to participate in MG support activities as this causes battery damage from frequent transitions. As a result, the RER value increases and the preference decreases. This can also be examined for the alternative situation.

In order to prolong the life of the battery by reducing the number of transition cycles, the value of RER regarding STP will be chosen. PoP is calculated using historical EV grid support participation trends as well as correlations between the other factors. Laxity mimics an EV's adaptable time frame for participating in grid support. These two decision-making factors aid in maximizing the use of EV storage, and in this situation, the RER is exactly proportionate. In this part, the estimation of STP and PoP is covered. Eq. (1) mentioned in Section 2 is used to estimate the value of Laxity. By mapping inputs to outputs (rank) based on the prior description of how each input affects the grid support and battery health, we establish a fuzzy rule basis. The rule base was developed with the intuitive notion of mapping as if the MG operator were to choose the EVs in the current time and situation. Later, a synthetic data set created using this fuzzy rule basis is utilized to train an intelligent CNN for RER. Table 1 (training data for CNN) has been collected from the sample fuzzy rule base provided below [36] using artificial training data.

Table 2
Sample data set for CNN training.

S. N0	DoD	Laxity	PoP	STP	rank
1	0.600	0.795	0.823	0.025	0.145
2	0.614	0.316	0.099	0.797	0.472
3	0.592	0.514	0.086	0.619	0.503
4	0.062	0.256	0.682	0.159	0.010
5	0.012	0.249	0.165	0.514	0.698
6	0.189	0.765	0.844	0.838	0.809
7	0.956	0.480	0.350	0.429	0.050
8	0.684	0.285	0.841	0.863	0.990
9	0.736	0.274	0.234	0.058	0.958
10	0.558	0.988	0.695	0.404	0.569
11	0.225	0.713	0.742	0.834	0.207
12	0.278	0.818	0.855	0.202	0.044
13	0.325	0.548	0.750	0.887	0.964
14	0.272	0.962	0.043	0.908	0.266
15	0.328	0.145	0.912	0.635	0.663
16	0.555	0.949	0.830	0.350	0.841
17	0.194	0.301	0.945	0.363	0.474
18	0.889	0.426	0.771	0.838	0.272
19	0.059	0.714	0.665	0.933	0.611
20	0.106	0.963	0.008	0.323	0.528

Table 3
Sample of past data of EV participation in V2G/G2V/IDL.

S. No	*SoC*	$\mathscr{L}$	*DoW*	*T*	$_S t$
1	0.82	0.15	0.40	0.49	0
2	0.87	0.14	0.08	0.49	0
3	0.08	0.87	0.24	0.34	1
4	0.40	0.58	0.12	0.90	1
5	0.26	0.55	0.18	0.37	−1
6	0.80	0.14	0.24	0.11	−1
7	0.43	0.85	0.42	0.78	0
8	0.91	0.62	0.05	0.39	1
9	0.18	0.35	0.90	0.24	−1
10	0.26	0.51	0.94	0.40	0

DoD	Laxity	PoP	STP	Rank
{'VH'}	{'M' }	{'VL'}	{'VH'}	{'H' }
{'H' }	{'H' }	{'VL'}	{'VH'}	{'H' }
{'VL'}	{'M' }	{'VH'}	{'VL'}	{'VL'}
{'VL'}	{'M' }	{'VL'}	{'H' }	{'VH'}
{'VL'}	{'M' }	{'VL'}	{'H' }	{'VH'}
{'VL'}	{'VH'}	{'VH'}	{'VH'}	{'VH'}
{'VH'}	{'H' }	{'M' }	{'H' }	{'VL'}
{'VH'}	{'M' }	{'VH'}	{'VH'}	{'VH'}
{'VH'}	{'M' }	{'M' }	{'VL'}	{'VH'}
{'H'}	{'VH'}	{'VH'}	{'H' }	{'H' }
{'M'}	{'VH'}	{'VH'}	{'VH'}	{'M' }
{'M'}	{'VH'}	{'VH'}	{'M' }	{'VL'}
{'M'}	{'H' }	{'VH'}	{'VH'}	{'VH'}
{'M'}	{'VH'}	{'VL'}	{'VH'}	{'M' }

9.1. Intelligent CNN for EV recommendation (RER)

Traditionally, intelligent CNNs [37] have been used for image-processing applications including object detection and categorization. Their architecture, however, may be modified for several kinds of data, including time series and text data, making them appropriate for a variety of applications. Intelligent networks must be translated into the proper format in order to be used with non-image input. For example, time series data can be turned into a 2D array by treating each data point as a pixel and each time step as a row, while text data can be converted into a 2D matrix by expressing each word as a vector and organizing

Table 4
Pearson correlation coefficients.

$\dot{r}$	*SoC*	$\mathscr{L}$	*DoW*	*t*	$_S t$
SoC	1.00				
$\mathscr{L}$	−0.58	1.00			
DoW	−0.50	−0.04	1.00		
T	−0.04	0.38	−0.22	1.00	
$_S t$	**0.07**	**0.51**	**−0.39**	**0.52**	**1.00**

Table 5
Performance of ANFIS to estimate PoP.

S. No	SoC	$\mathscr{L}$	DoW	t	PoP
1	0.77	0.44	0.20	0.68	**0.5480**
2	0.40	0.83	0.41	0.50	**0**
3	0.81	0.77	0.75	0.19	**0**
4	0.76	0.17	0.83	0.50	**0**
5	0.38	0.86	0.79	0.15	**0**
6	0.22	0.99	0.32	0.05	**0**
7	0.79	0.51	0.53	0.85	**0**
8	0.95	0.88	0.09	0.56	**0**
9	0.33	0.59	0.11	0.93	**0.5711**
10	**0.67**	**0.15**	**0.14**	**0.70**	**0.0120**

them according to their order in the text. Following data transformation, a CNN can be trained utilizing similar methods to those used for picture data. In order to produce predictions or choices based on the input, the CNN will learn to recognize patterns and characteristics in the data. An intelligent CNN, for instance, can be used to analyse sensor data from a manufacturing facility to find patterns that point to equipment failure or service requirements. On the basis of real-time sensor data, the CNN can be trained using historical sensor data to forecast when maintenance is necessary. By converting the data into an appropriate format and teaching the CNN to spot patterns and features in the data, CNNs are a flexible tool that may be used for selection criteria based on non-image data. This broadens the variety of uses for CNNs beyond the conventional image processing tasks listed in Table 2.

9.2. Probability of participation

Through V2G and G2V features, historical data on EV participation in grid support activities can be used to assess the probability of participation (PoP). The history of owner involvement in grid support has been taken into consideration in this study to identify patterns of behavior that correlate with various parameters, including SoC, laxity ($\mathscr{L}$), Day of the Week (DoW), and time interval (t). With the help of this information, the probability that an EV is in the V2G/G2V, or IDL states may be calculated.

9.2.1. Correlation

The input data, which consists of SoC, L, DoW, and t, has been associated with the state in Table .3 in order to estimate PoP. In this case, the EV status, S^t, is either −1 for V2G, +1 for G2V, or 0 for IDL. The correlation has been utilized in this section to assess the link between the variables listed in Table 2. Correlation aids in decision-making by assessing the relationship between the choice and input variables. We can maximize the use of EV storage in this situation by knowing the feature behavior of the EV owner (PoP). A numerical indicator of how closely the variables are related is the correlation coefficient (r). The formula is given by Eq. (40), and the Pearson Correlation Coefficient is used to assess the linear relationship between the data variables. These coefficients (r), which are displayed in Table .4, were extracted using MS-Excel and the data analysis tool bundle. The value of r falls between −1 and 1, where −1 denotes pure negativity and +1 denotes pure positivity. The correlation between the variables is zero, or 0. The training data for ANFIS created for EV prioritizing is prepared using the

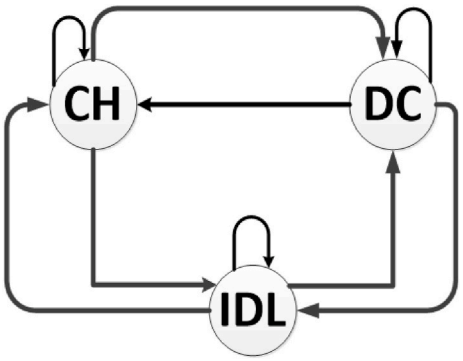

Fig. 8. Chances of state transition for an EV.

correlation between the factors to map the input and decision variables. On the other hand, if we want to swap out ANFIS for a fuzzy controller to estimate the PoP, the same can also be utilized to construct the fuzzification rule basis.

$$\dot{\mathbf{r}} = \frac{\{\mathbf{n}\sum(\mathrm{xy}) - (\sum(\mathbf{x}) * \sum(\mathbf{y}))\}}{\left\{\sqrt{\mathbf{n}\sum\mathbf{x^2} - (\sum\mathbf{x})^2}\right\} - \left\{\sqrt{\mathbf{n} * \sum\mathbf{y^2} - (\sum\mathbf{y})^2}\right\}} \tag{40}$$

9.3. PoP estimation using ANFIS

With four input variables and one output (St) in this method, ANFIS is trained using the data in Table 5. Five input membership functions plus 1-output membership function are employed in the Sugeno-type fuzzy inference system (triangular. All parameters for input and output are transformed into per-unit values using Equation 6.1. The membership function values in use range from 0 to 1. The hybrid training technique used in this work has 100 epochs and a 0.005 error tolerance. The ANFIS is trained using 90 % of the training data provided in Table 1 in this study, with the remaining 10 % being used for testing. In Table 4, the ANFIS's operation is shown. The value of PoP in Table 4 ranges from −1 to 1. Here, '0′ denotes the idle state of the EV, '-ve' denotes the likelihood of G2V, and '+ve' denotes the probability of V2G by the given EV during the given time frame.

9.4. STP estimation

It is advised to extend the battery state for the alternative periods, prioritizing maximal EV storage consumption while reducing mode transitions, to optimize quick changes between V2G and G2V and minimize battery deterioration is shown in Fig. 8). To do this, the SoC, current mode, zone transition probability, zone type, and EV availability probability are combined to determine the EV utility rate for the following two intervals. As a result, the EV experiences three states at each time interval, with the likelihood of a state shift as shown in Fig. 9. Fig. 9 displays the likelihood of zones transitioning across 96 intervals.

(a) ***Transition probability 'CH →CH', p^t_{11}:***

To estimate the STP for the next interval we formulate the probabilistic equations that use the following terms.

$p^{ch,t+1}_{j,SoC}$ = probobility of going to be in charging mod at t + 1

$p^{dc,t+1}_{j,SoC}$ = probobility of going to be in discharging mod at t + 1

p^{t+1}_{11} = probobility of going to be in discharging mod at t + 1′*given that the EV is in charging mode during* '*t*'

Here, 1, 2, and 3 represent charging, discharging, and idle modes

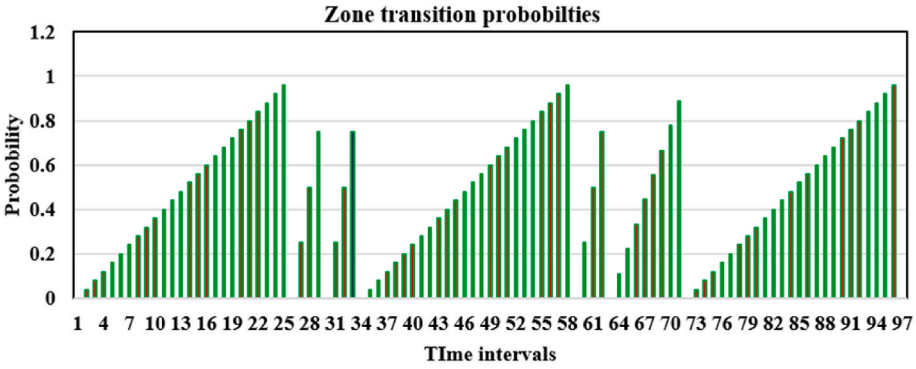

Fig. 9. Zone transition probabilities over 96 intervals.

respectively. So, $p_{12}^{t+1}, p_{31}^{t+1}$ and so on can be understood what they represent.

$p_{j,avail}^{t+1}$ = available probability of EV at t + 1

p_z^{t+1} = zone transition probability at t + 1. These terms are also represented by 't' interval.

$$P_{j,1}^{t+1} = \frac{P_{j,SoC}^{ch,t+1} * P_{j,avl}^{t+1}}{P_{avl}^{t}} = \frac{\left(1 - \left(SoC_j^t + \Delta Soc_j\right)\right)}{P_{avl}^{t}} \tag{41}$$

Here, p_z^{t+1} is the probability of zone change over or zone transition either from charging zone to discharging zone or vice-versa. The vector transition probabilities are defined by the vector $p_z = [\, p_z^1 \;\; p_z^2 \; p_z^3 \;\; p_z^4 \;\;\; p_z^5 \ldots\ldots\ldots p_z^{96}]$ as per Fig. 1.

$$P_{11}^{t+1} = \frac{\left(1 - \left(SoC_j^t + \Delta Soc_j\right)\right) * P_{avl}^{t+1}}{P_{avl}^{t}} * \left(1 - P_z^{t+1}\right) \tag{42}$$

Where $\Delta SoC_j = \frac{P_{evj}^{rate} * \eta \Delta t}{E_j}$.

(b) ***Transition probability 'CH → DC', p_{12}^t:***

$$P_{j,2}^{t+1} = \frac{P_{SoC}^{ch,t} * P_{avl}^{t+1}}{P_{avl}^{t+1}} = \frac{\left(\left(SoC_j^t + \Delta Soc_j\right) * P_{avl}^{t+1}\right)}{P_{avl}^{t}} \tag{43}$$

Here, the transition probability is determined using Eq. (44) with the use of zone transition probability.

$$P_{1,2}^{t+1} = \frac{\left(1 - \left(SoC_j^t + \Delta Soc_j\right)\right) * P_{avl}^{t+1}}{P_{avl}^{t}} * \left(P_z^{t+1}\right) \tag{44}$$

(c) ***Transition probability 'CH → IDL', p_{13}^t:***

$$P_{j,3}^{t+1,idl} = \left(SoC_j^t + \Delta SoC_j\right) \tag{45}$$

$$P_{j,13}^{t+1,idl} = \left(SoC_j^t + \Delta SoC_j\right) * \left(1 - P_z^{t+1}\right) \tag{46}$$

$$P_{j,13}^{t+1,idl} = \left(\left(SoC_j^t + \Delta SoC_j\right) - Z_{12}^{t+1}\right) * \left(1 - \left(1 - Z_{12}^{t+1}\right) * P_z^{t+1}\right) \tag{47}$$

Here, $Z_{12}^{t+1} = 1$; if zone changes from CH to DC.
$Z_{12}^{t+1} = -1$; if zone changes from DC to CH.
$Z_{12}^{t+1} = 0$; if there is no zone transition.

(d). Transition probability 'DC → CH', p_{21}^t:

$$P_{j,1}^{t+1} = \frac{P_{soc}^{dc,t} * P_{avl}^{dc,t}}{P_{avl}^{t}} = \frac{\left(1 - \left(SoC_j^t - \Delta Soc_j\right)\right)}{P_{avl}^{t}} * \left(P_{avl}^{t+1}\right) \tag{48}$$

$$P_{21}^{t+1} = \frac{\left(1 - \left(SoC_j^t - \Delta Soc_j\right)\right) * P_{avl}^{t+1}}{P_{avl}^{t}} * \left(P_z^{t+1}\right) \tag{49}$$

(e) ***Transition probability 'DC →DC', p_{22}^t:***

$$P_{j,u,2}^{t+1} = \frac{P_{j,soc}^{dc,t+1} * P_{j,avl}^{t+1}}{P_{avl}^{t}} = \frac{\left(\left(SoC_j^t - \Delta Soc_j\right)\right)}{P_{avl}^{t}} * \left(P_{avl}^{t+1}\right) \tag{50}$$

$$P_{22}^{t+1} = \frac{\left(\left(SoC_j^t - \Delta Soc_j\right)\right) * P_{avl}^{t+1}}{P_{avl}^{t}} * \left(1 - P_z^{t+1}\right) \tag{51}$$

(f) ***Transition probability 'DC → IDL', p_{23}^t:***

$$P_{j,3}^{t+1,idl} = \left(1 - \left(SoC_j^t - \Delta Soc_j\right)\right) \tag{52}$$

$$P_{j,23}^{t+1,idl} = \left(1 - \left(SoC_j^t - \Delta Soc_j\right)\right) * \left(1 - P_z^{t+1}\right) \tag{53}$$

If the zone transition is from DC→ CH, the probability that EV will be in an idle state cannot be directly realized using (54)

$$P_{j,23}^{t+1,idl} = \left(1 - \left(SoC_j^t - \Delta SoC_j\right) + Z_{12}^{t+1}\right) * \left(1 - \left(1 - Z_{12}^{t+1}\right) * P_z^{t+1}\right) \tag{54}$$

(g) ***Transition probability 'IDL → CH', p_{31}^t.***

If the next zone transition is DC→CH:

The transition probability is given by (55) if the zone transition is DC→CH. $Z_{12}^{t+1} = -1$.

$$P_{j,23}^{t+1,idl} = \left(\left(Z_{12}^{t+1} + SoC_j\right)\right) * \left(1 - \left(1 - Z_{12}^{t+1}\right) * P_z^{t+1}\right) \tag{55}$$

If the next zone transition is CH→DC:

$$P_{j,31}^{t+1,idl} = \left(\left(Z_{12}^{t+1} - SoC_j\right)\right) * \left(\left(1 - Z_{12}^{t+1}\right) * P_z^{t+1}\right) \tag{56}$$

(h) ***Transition probability 'IDL→ DC', p_{32}^t:***

If there is a zone transition from CH to DC, then the transition probability from idle to discharging depends on $\{SoC_j^t\}$.

The transition probability is given by (57) if the zone transition is CH→DC. $Z_{12}^{t+1} = 1$.

$$P_{j,32}^{t+1,idl} = \left(\left(1 - Z_{12}^{t+1} + SoC_j\right)\right) * \left(1 - \left(1 - Z_{12}^{t+1}\right) * P_z^{t+1}\right) \tag{57}$$

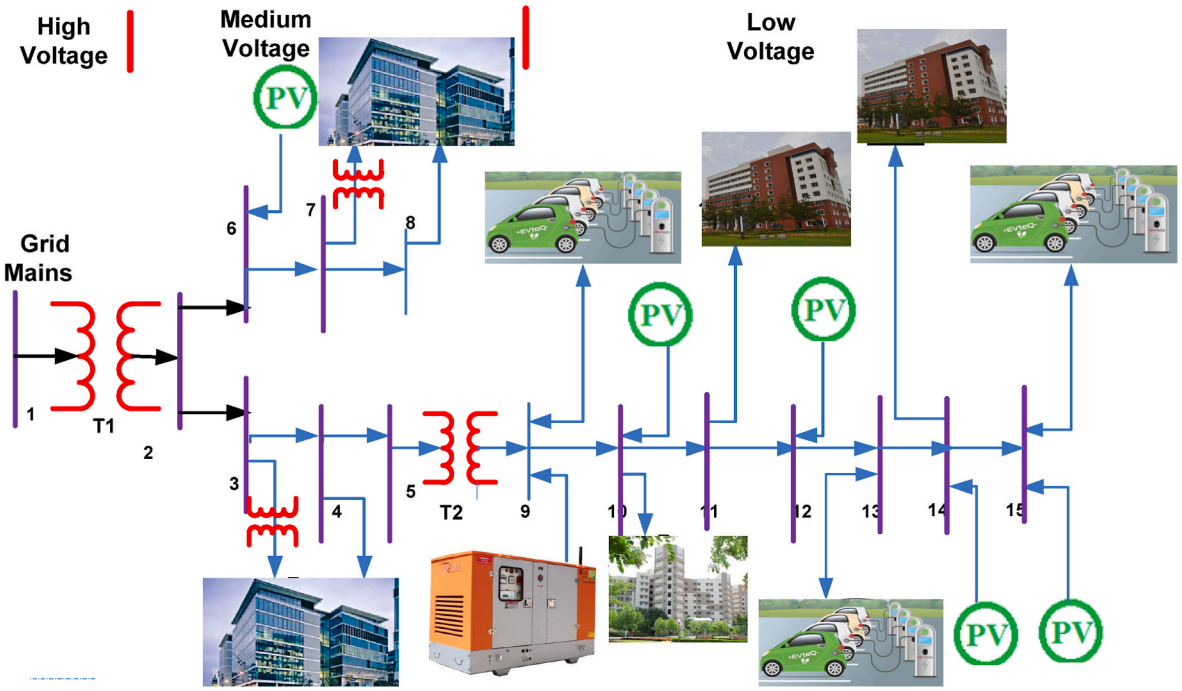

Fig. 10. Line diagram of MG.

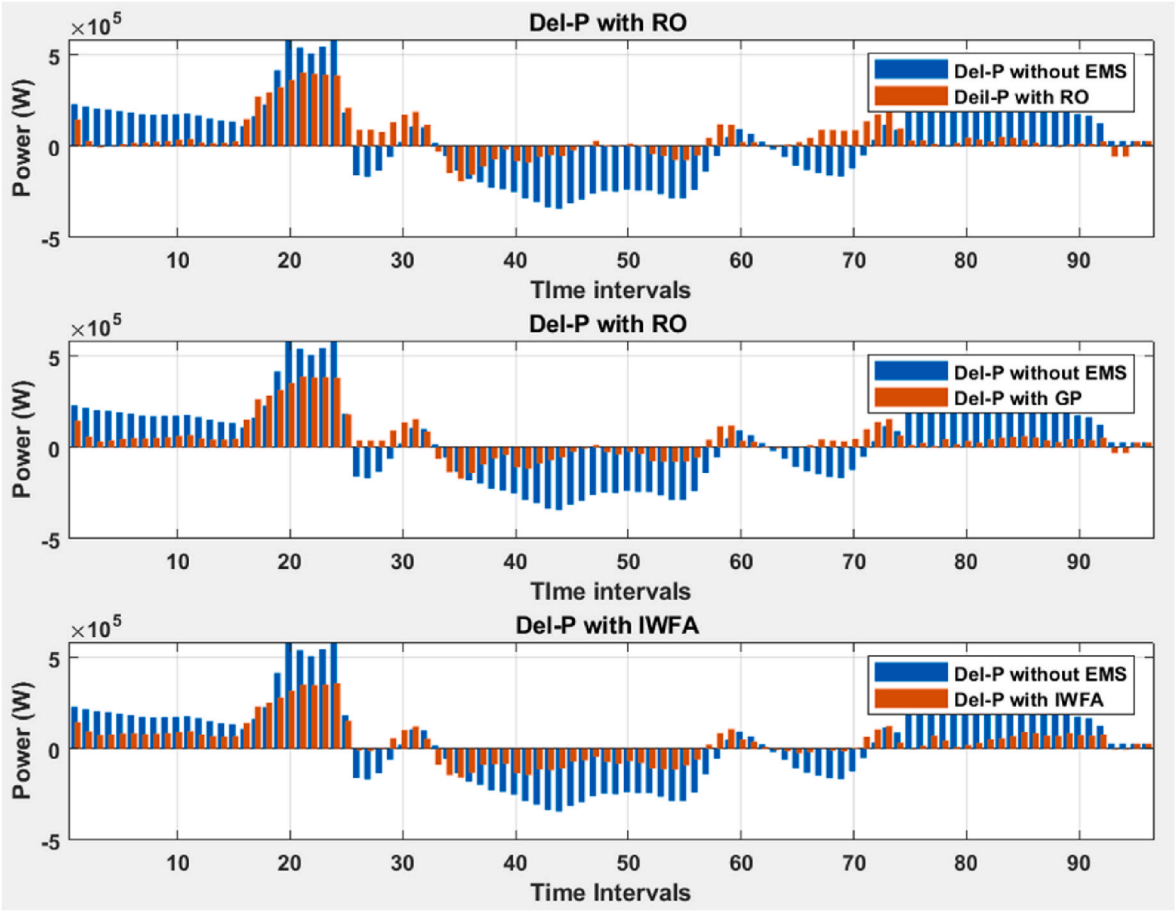

Fig. 11. Comparison of three methods for OAES in terms of deviation from max demand.

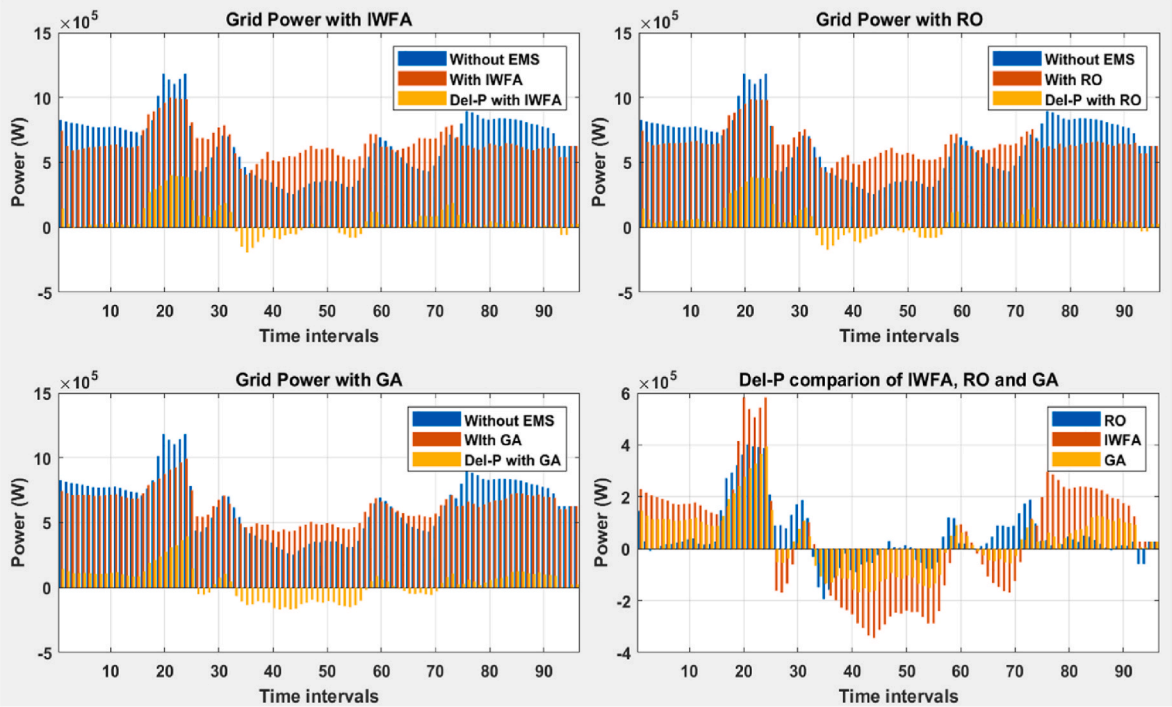

Fig. 12. Comparison of three methods for OAES in terms of grid power.

The shift from idle to discharging mode won't occur if the following zone transfer is from DC to CH because it is preferable to use EVs in charging mode in the CH zone. It is evident that the EV will not be used in discharging mode despite having some SoC of 0.8 at the CH zone. Consequently, in this scenario, the transition probability will be equal to 0.

$$P_{j,32}^{t+1,idl} = \left(\left(Z_{12}^{t+1} + SoC_j\right)\right) * \left(\left(1 + Z_{12}^{t+1}\right) * P_z^{t+1}\right) \quad (58)$$

Where $Z_{12}^{t+1} = -1$.

(i) ***Transition probability 'IDL →IDL', p'_{33}.***

If there is no zone transition, then the EV will remain to stay in the idle position in t+1 if it was in the idle position in interval t. If the next zone transition is CH→DC:

If there is no zone transition, i.e., $p_z^{t+1} = 0$, then, $p_{33}^{t+1} = 1$.

$$\text{Else if}, p_z^{t+1} = 1, p_{33}^{t+1} = \left(1 - P_{32}^{t+1}\right) \quad (59)$$

Here, $p_{32}^{t+1,idl}$ is the transition probability from IDL→DC

$$\text{Else if}, p_z^{t+1} = 1, p_{33}^{t+1} = \left(1 - P_{31}^{t+1,idl}\right) \quad (60)$$

Here, $p_{31}^{t+1,idl}$ is the transition probability from IDL→DC.

The (35) represents the transition probability from i → j after the next two intervals i.e., at the time (t+1) and that of at (t+2) the transition probability is represented by (37).

$$p_{ij}^{t+1} = \sum_{k=1}^{3} P_{ik}^{ch} P_{kj}^{ch} \quad (61)$$

$$p_{13}^{t+2} = \sum_{k=1}^{3} \left(P_{ik}^{ch} \sum_{l=1}^{3} P_{kl}^{ch} P_{lj}^{ch}\right. \quad (62)$$

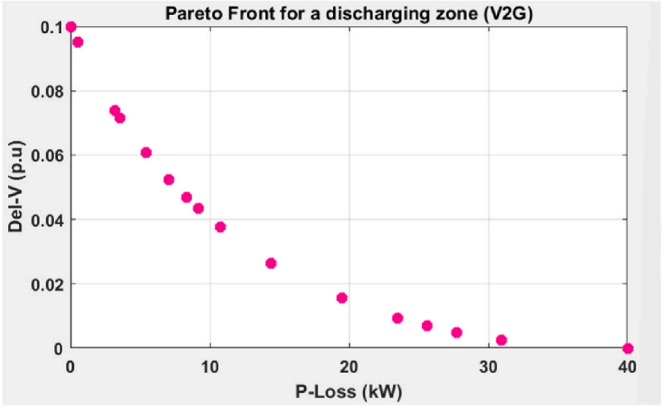

Fig. 13. Pareto front for selection of OPA.

10. Results and discussions

The suggested course of action is put into action in the MG scenario using a variety of energy sources, including solar PV, wind, fuel cells, and EV fleets. It is implemented in a smart grid simulation environment powered by MATLAB [38] (Fig. 10). The suggested EMS has been examined in several circumstances in this section. The main conclusions will be more focused on the goals of min, ΔP, ΔV, grid energy cost, and EV battery degradation. Results from various examples have been used to examine the effects of each stage in the proposed EMS on the aforementioned objectives. The highest demand that is agreed upon from the main grid is 850 kVA apparent power, in our opinion. Note that we did not consider the best deal for the highest demand from the grid, thus this number is not optimal. However, we chose three situations with maximum demands of 800 kWh, 850 kWh, and 900 kWh for a random comparison. According to the power pricing structure in India, the cost estimates and penalty restrictions have been explained in Section 2.

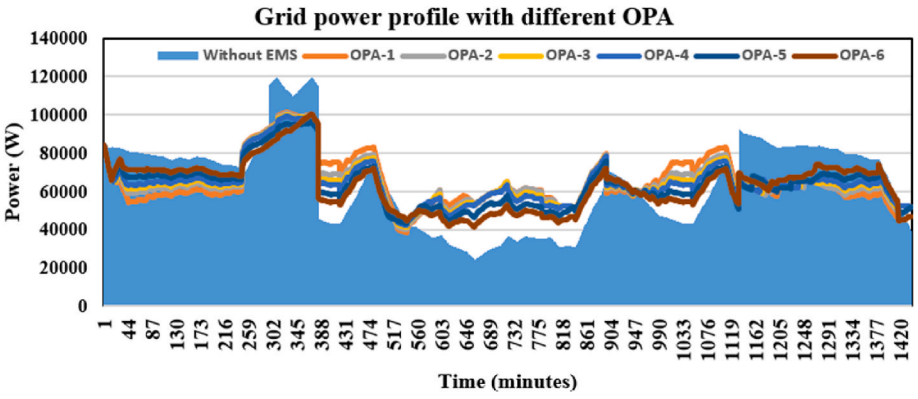

Fig. 14. Comparison of the impact of multiple OPA selections on grid power profile.

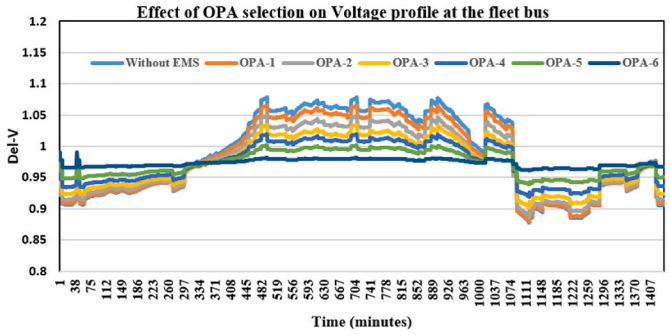

Fig. 15. Comparison of impact of multiple OPA selection on Voltage profile at the fleet bus.

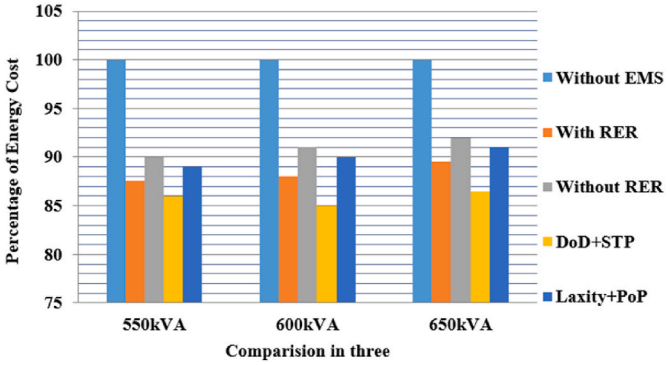

Fig. 17. Cost comparison among EMS, RER, and decision variables.

Table 6
Cost comparison among EMS, OPA, and RER.

Max Demand from Grid (% cost)	800kVA	850kVA	900kVA
Without EMS	100	100	100
With EMS	87.6	88	89.5
Without OPA	91	91.8	93
Without RER	90	91	92

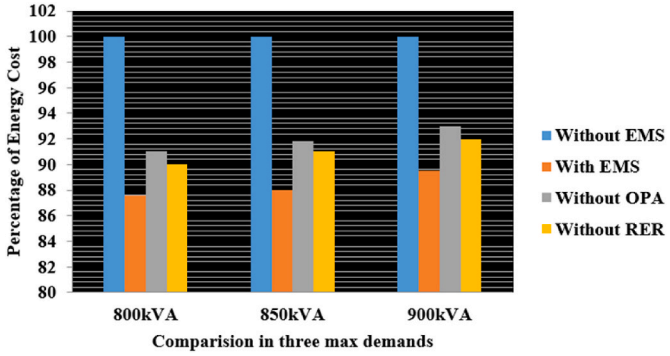

Fig. 16. Cost comparison among EMS, OPA, and RER.

10.1. Comparison of OAES

Three distinct techniques have been used to distribute the energy throughout the intervals. Here, we contrast these three approaches based on the actual power being exchanged between MG and EVs (in Fig. 3) and the grid power divergence from 850 kVA (Fig. 11). According to the discussion in section 3, the expected energy demand (MWh) in

Table 7
impact of individual decision variable of RER on cost variation.

Max Demand from Grid (% cost)	800kVA	850kVA	900kVA
Without EMS	100	100	100
With RER	87.6	88	89.5
Without RER	90	91	92
DoD + STP	86	85	86.5
Laxity Pop	89	90	91

seven zones is: 1.6, −0.14, 0.07, −1.5, 0.06, −0.25 and 1.08. The actual energy distribution (MWh) determined by OAES using IWFA is as follows: 1.01, −0.03, 0.06, −0.42, 0.05, −0.03, and 0.38. In this case, - denotes the charging zone and +, the discharging zone. According to the comparison analysis, the divergence from 850kVA is predicted to be at its lowest point when we utilize IWFA, followed by RO, and at its highest point when we use GP. The same information is shown in Figs. 11 and 12, where three techniques have been contrasted in terms of the quantity of power coming from EVs that is being transferred.

10.2. Impact of OPA selection

In continuation to section 4 from which we obtain the Pareto-front solution for OPA, here we present the analysis part on how the selection of OPA will impact the voltage and grid power deviation. It can be observed from Fig. 14 for OPA-1, OPA-2, …. … and OPA-6. The process of selecting the OPA from the Pareto-front for power loss and voltage deviation was thoroughly examined. The proposed solutions (OPAs from the pareto front) were compared by selecting different OPA options from the Pareto-front, as shown in Fig. 13. As the power transactions between the fleet and grid can cause voltage variation, it is essential to set a power transaction limit to control this deviation. As shown in Figs. 14

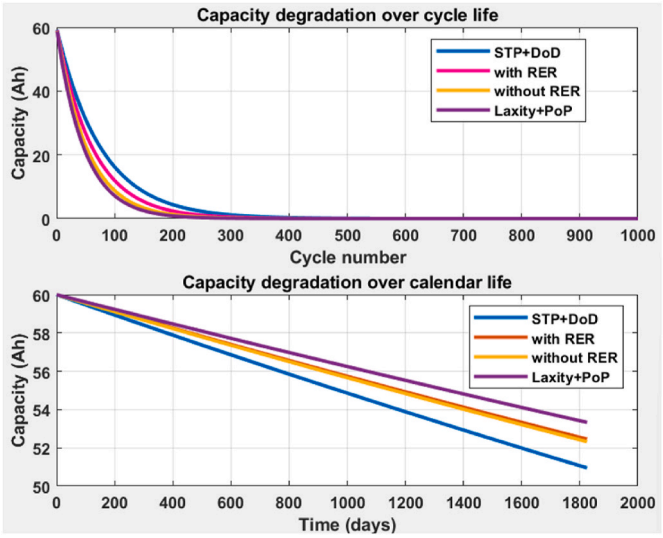

Fig. 18. Battery longevity due to RER and its decision variables.

and 15, choosing OPA from the Pareto-front significantly affects voltage deviation and load flattening. Additionally, using this strategy makes it easier to regulate both frequency and voltage. Fig. 15 shows the voltage variations and illustrates the effectiveness of the suggested method for controlling the voltage deviation. Additionally, the impact of varying charging and discharging rates on EVs was examined while accounting for battery degeneration. It's crucial to remember that this approach assumes fixed power EVs for V2G G2V power transfers.

10.3. Grid power cost

In this part, using Fig. 17 and Table .6, we analyse the variation in grid power costs under various conditions, including those with and without EMS, RER, and OAES. Fig. 2 shows the effects of each choice variable in RER. In order to compare costs, we use the cost at the maximum demand of 850 kVA (100 %) as the baseline. OPA's impact is more significant than RER's since RER only weighs battery longevity in half (Fig. 16). It is because one of the goals of the MOOP, for which OPA is chosen, is to minimize losses. However, the choice of OPA from the Pareto-front solution set will directly affect cost variation. Cost reduction results from a compromise on ΔV, and vice versa. Fig. 17 shows how the RER's individual decision variable affects cost variation. The similar thing can be seen in Table 7, too. While STP and DoD will almost certainly be in the exact opposite situation, decision variables Laxity and PoP will demonstrate a direct impact on costs. In the worst-case scenario, cost is increased if we only consider DoD & STP as the choice variables for RER. In the best-case situation, cost is minimized if only DoD & STP are the decision variables. The cost is moderate and falls in between the situations of RER and without EMS when all four choice variables are taken into account.

10.4. Impact of RER and decision variables

The impact of V2G plus G2V on battery life is explored in this section, as it was in Section 2. It is commonly known that the battery SoH depends on a number of variables, although an accurate estimate is neither predicted nor possible. Here, we take into account the battery's deterioration in terms of both calendar and cycle lifetimes. We estimate the capacity deterioration using the equations Eq. (39) and (40), despite the fact that doing so is highly difficult and impossible. In contrast to Laxity and PoP, decision variables (STP and DoD) in RER will directly affect capacity fading in this situation. In Fig. 18, we examine the capacity fading over the cycle and calendar file for four situations (with RER, without RER, with DoD & STP, and without DoD & STP). In the worst case situation, capacity fading is leveraged if DoD & STP are not taken into account while making decisions for RER. In the best case scenario, DoD & STP are the only factors taken into consideration. When all four RER decision variables are taken into account, the fading is moderate and less severe than the worst-case scenario, as shown in Fig. 18

11. Conclusion

An innovative EMS for MG with grid support was suggested in the article. The goal was to use RES and EV storage to lessen reliance on the grid. The proposed EMS had three execution phases: OAES, OPF, and RER. The estimated storage need (kWh/t) is based on the predicted demand and RES and is based on dividing the 24-h period into 96 time intervals (t). They established the required amount of storage and the charging and discharging time zones (G2V and V2G, respectively). The main goal is "load flattening," which aims to lessen the MG's reliance on the grid. Three approaches were first used to obtain OAES, but the OAIWF algorithm performed the best. Based on OAES, OPF was obtained for each "t" by resolving a MOOP with the dual goals of reducing voltage variation and network power loss. The OPF for the fleet was derived for each "t" from the Pareto-front, where we took into account a solution that improves performance while still achieving both MOOP goals. The CNN was trained using the information obtained from the fuzzy rule base in the third stage, which comprised four decision variables as inputs and the rank of EV as an output. During this phase, the key goals were to avoid battery deterioration and optimize its use for MG support. A MATLAB-based smart grid system with heterogeneous entities was used to implement the suggested EMS, and various case studies were examined. Different combinations of CNN inputs have been used to study the effects of decision variables in RER. It has been researched how the Pareto-front choice affects voltage and power loss.

Funding statement

This work was supported in part by the Canada National Sciences and Engineering Research Council through the Laval University, Grant ALLRP567550-21.

CRediT authorship contribution statement

Hussaian Basha CH: Conceptualization, Methodology, Software. **Ramakrishna Reddy K:** Conceptualization, Methodology, Software. **Dhanamjayulu C:** Writing – original draft, Visualization, Investigation, Writing – original draft, Visualization, Investigation, Supervision, Software, Validation, Writing- Reviewing and Editing. **Innocent Kamwa:** Supervision, Software, Validation, Writing- Reviewing and Editing, Funding acquisition. **S.M. Muyeen:** Supervision, Software, Validation, Writing- Reviewing and Editing, Funding acquisition.

Declaration of competing interest

The authors declare that they have no known competing financial interests or personal relationships that could have appeared to influence the work reported in this paper.

Data availability

No data was used for the research described in the article.

Acknowledgment

This work was supported in part by the Canada National Sciences and Engineering Research Council through the Laval University, Grant ALLRP567550-21.

References

[1] M. Lonkar, S. Ponnaluri, An Overview of DC microgrid operation and control, in: Proceedings of the IREC2015 the Sixth International Renewable Energy Congress, Sousse, Tunisia, 24–26 March 2015, IEEE, Piscataway, NJ, USA, 2015, pp. 1–6.

[2] D. Magdefrau, T. Taufik, M. Poshtan, M. Muscarella, Analysis and review of DC microgrid implementations, in: Proceedings of the 2016 International Seminar on Application for Technology of Information and Communication (ISemantic), Semarang, Indonesia, 5–6 August 2016, IEEE, Piscataway, NJ, USA, 2016, pp. 241–246.

[3] D. Kumar, F. Zare, A. Ghosh, DC microgrid technology: system architectures, AC grid interfaces, grounding schemes, power quality, communication networks, applications, and standardizations aspects, IEEE Access 5 (2017) 12230–12256.

[4] M.A. Sofla, G.B. Gharehpetian, Dynamic performance enhancement of microgrids by advanced sliding mode controller, Int. J. Electr. Power Energy Syst. 33 (2011) 1–7.

[5] S. Phommixay, M.L. Doumbia, L. Lupien St-Pierre, Review on the cost optimization of microgrids via particle swarm optimization, Int. J. Energy Environ. Eng. 11 (2020) 73–89.

[6] L. Shi, Y. Luo, G. Tu, Bidding strategy of microgrid with consideration of uncertainty for participating in power market, Int. J. Electr. Power Energy Syst. 59 (2014) 1–13.

[7] C. Li, F. De Bosio, S.K. Chaudhary, M. Graells, J.C. Vasquez, J.M. Guerrero, Operation cost minimization of droop-controlled DC microgrids based on real-time pricing and optimal power flow, in: Proceedings of the IECON 2015—41st Annual Conference of the, IEEE Industrial Electronics Society, Yokohama, Japan, 9–12 November 2015 003905, 003909.

[8] X. Qian, Y. Yang, C. Li, S.C. Tan, Operating cost reduction of DC microgrids under real-time pricing using adaptive differential evolution algorithm, IEEE Access 8 (2020) 169247–169258.

[9] K. Zhang, L. Xu, M. Ouyang, H. Wang, L. Lu, J. Li, Z. Li, Optimal decentralized valley-filling charging strategy for electric vehicles, Energy Convers. Manag. 78 (2014) 537–550.

[10] S. Rehman, H.U.R. Habib, S. Wang, M.S. Büker, L.M. Alhems, H.Z. Al Garni, Optimal design and model predictive control of standalone HRES: a real case study for residential demand side management, IEEE Access 8 (2020) 29767–29814.

[11] M. Hannan, F. Azidin, A. Mohamed, Multi-sources model and control algorithm of an energy management system for light electric vehicles, Energy Convers. Manag. 62 (2012) 123–130.

[12] Q. Zhang, K.N. Ishihara, B.C. Mclellan, T. Tezuka, Scenario analysis on future electricity supply and demand in Japan, Energy 38 (2012) 376–385.

[13] A. Zakariazadeh, S. Jadid, P. Siano, Stochastic multi-objective operational planning of smart distribution systems considering demand response programs, Elec. Power Syst. Res. 111 (2014) 156–168.

[14] B.S.M. Borba, A. Szklo, R. Schaeffer, Plug-in hybrid electric vehicles as a way to maximize the integration of variable renewable energy in power systems: the case of wind generation in northeastern Brazil, Energy 37 (2012) 469–481.

[15] Z. Ma, D.S. Callaway, I.A. Hiskens, Decentralized charging control of large populations of plug-in electric vehicles, IEEE Trans. Control Syst. Technol. 21 (2013) 67–78.

[16] L. Yao, Z. Damiran, W.H. Lim, Optimal charging and discharging scheduling for electric vehicles in a parking station with photovoltaic system and energy storage system, Energies 10 (2017) 550 [CrossRef]).

[17] T.P. Hai, H. Cho, I.Y. Chung, H.K. Kang, J. Cho, J. Kim, A novel voltage control scheme for low-voltage DC distribution systems using multi-agent systems, Energies 10 (2017) 41.

[18] ANSI C84 1-2011. American National Standard for Electric Power Systems and Equipment-Voltage Ratings (60 Hertz), National Electrical Manufacturers Association: Rosslyn, VA, USA, 2011.

[19] T.P. Hai, I.Y. Chung, T.H. Kim, J. Juyong Kim, Coordinated voltage control scheme for multi-terminal low-voltage DC distribution system, J. Electr. Eng. Technol. 13 (2018) 1459–1473.

[20] K. Mahmoud, M. Abdel-Nasser, E. Mustafa, Z.M. Ali, Improved salp-swarm optimizer and accurate forecasting model for dynamic economic dispatch in sustainable power systems, Sustainability 12 (2) (2020) 576.

[21] Amit Kumar, Prerna Jain, Satish Sharma, Transactive energy management for microgrids considering techno-economic perspectives of utility–a review, Int. J. Energy Res. 46 (2022) 16127–16149, 12.

[22] Seyed Hasan Mirbarati, et al., Techno-economic-environmental energy management of a micro-grid: a mixed-integer linear programming approach, Sustainability 14 (2022) 15036, 22.

[23] Yang Bao, et al., Optimal planning and multi-criteria decision making for effective design and performance of hybrid microgrid integrated with energy management strategy, Sustain. Energy Technol. Assessments 56 (2023) 103074.

[24] Sk A. Shezan, et al., Selection of the best dispatch strategy considering techno-economic and system stability analysis with optimal sizing, Energy Strategy Rev. 43 (2022) 100923.

[25] Reza Saki, et al., Interactive Multi-level planning for energy management in clustered microgrids considering flexible demands, Int. J. Electr. Power Energy Syst. 138 (2022) 107978.

[26] Seyed Ehsan Ahmadi, et al., Multi-objective stochastic techno-economic-environmental optimization of distribution networks with G2V and V2G systems, Elec. Power Syst. Res. 218 (2023) 109195.

[27] Zi-Xuan Yu, et al., Techno-economic planning and operation of the microgrid considering real-time pricing demand response program, Energies 14 (2021) 4597, 15.

[28] Reza Khalili, et al., Robust multi-objective optimization for the Iranian electricity market considering green hydrogen and analyzing the performance of different demand response programs, Appl. Energy 334 (2023) 120737.

[29] Azam Salari, et al., Fuzzy Q-learning-based approach for real-time energy management of home microgrids using cooperative multi-agent system, Sustain. Cities Soc. 95 (2023) 104528.

[30] Shahab Eslami, et al., Integrating heat pumps into district heating systems: a multi-criteria decision analysis framework incorporating heat density and renewable energy mapping, Sustain. Cities Soc. 98 (2023) 104785.

[31] Ghazimirsaeid, Seyedeh Samaneh, et al., Multi-agent-based energy management of multiple grid-connected green buildings, J. Build. Eng. 74 (2023) 106866.

[32] C. Liu, S.S. Abdulkareem, A. Rezvani, S. Samad, N. Aljojo, L.K. Foong, K. Nishihara, Stochastic scheduling of a renewablebased microgrid in the presence of electric vehicles using modified harmony search algorithm with control policies, Sustain. Cities Soc. 3 (2020) 102183.

[33] M.H. Mostafa, S.H. Aleem, S.G. Ali, A.Y. Abdelaziz, P.F. Ribeiro, Z.M. Ali, Robust energy management and economic analysis of microgrids considering different battery characteristics, IEEE Access 18 (8) (2020) 54751–54775.

[34] A. Shayegan-Rad, A. Badri, A. Zangeneh, Day-ahead scheduling of virtual power plant in joint energy and regulation reserve markets under uncertainties, Energy 121 (2017) 114–125.

[35] R. Mkahl, A. Nait-Sidi-Moh, J. Gaber, M. Wack, An optimal solution for charging management of electric vehicles fleets, Elec. Power Syst. Res. 146 (2017) 177–188.

[36] J. Jannati, D. Nazarpour, Optimal energy management of the smart parking lot under demand response program in the presence of the electrolyser and fuel cell as hydrogen storage system, Energy Convers. Manag. 138 (2017) 659–669.

[37] J. Timpner, L. Wolf, Design and evaluation of charging station scheduling strategies for electric vehicles, IEEE Trans. Intell. Transport. Syst. 15 (2) (2013) 579–588.

[38] Rasmus Pedersen, et al., DiSC: a simulation framework for distribution system voltage control. European Control Conference (ECC), IEEE, 2015, 2015.